J Mater Sci (2010) 45:2372–2380
DOI 10.1007/s10853-009-4203-3

Morphology and mechanical properties of polyacrylonitrile/attapulgite nanocomposite

Han Yin · Huifang Chen · Dajun Chen

Received: 2 November 2009 / Accepted: 31 December 2009 / Published online: 14 January 2010

Abstract The major objective of this work is to understand the effects of attapulgite (AT) on the mechanical properties of polyacrylonitrile (PAN)/AT nanocomposite film. The well dispersed but irregularly distributed AT nanoparticles in the matrix was observed by scanning electron microscopy (SEM) and UV–vis spectra. The mechanical properties were investigated by means of tensile tests and dynamic mechanical analyses (DMA). The results showed that the incorporation of AT significantly improved the tensile strength and modulus of the PAN matrix. The fracture morphologies analysis has further suggested that small amount of AT nanorods may slide and orient along the tensile direction, resulting in homogenous stress transfer, thus increase the toughness of the PAN. However, the nanorods network formed in high AT content sample probably hindered the deformation of the matrix and generated the stress concentration points, leading to the remarkable increase of embrittlement of the samples. Following this concept, the volume of the constrained polymer chains was also calculated with DMA data and showed the good correlation with conclusion drawn in the tensile tests.

Introduction

Polymers filled with natural layered silicates, such as montmorillonite, kaolinite and mica, have attracted significant interests in the past decades and a large number of works in this field have been done. Actually it is well demonstrated that remarkable improvements in physico-chemical properties occur upon the formation of the polymer/clay nanocomposites [1]. From a morphological point of view, it is generally recognized that the dispersion of particles is closely related with the mechanical properties of final product and the exfoliated rather than intercalated silicate layers are considered as the ideal structure for high-performance composites. Nevertheless, the non-covalent bonding forces between clay sheets (such as electrostatic charge attraction, hydrogen bonding, and van der Waals forces) are always a big challenge in pre-treating of clay and processing of polymer/clay nanocomposite. To obtain the well exfoliated and dispersed layered clay sheets, various chemical and physical strategies have been adopted [2–5]. For example, in situ polymerization is a widely used method, in which inorganic particles are dispersed in a monomer and then polymerization of the reactive mixture is induced by heat treatment. With this method, inorganic particles can be homogeneously dispersed in polymer matrix, leading to the composites with enhanced mechanical and thermal properties.

In this study, we have investigated nanocomposites based on attapulgite (AT). As a native mineral, AT is characterized by a short fibrous morphology, which is resolved as a randomly oriented network of densely packed rods [6]. AT has primarily been used in various commercial fields, including rheological agents, absorbents, catalyst carrier [7–9]. In the recent development of nanocomposites, AT has also attracted growing interests due to its unusual rod-like geometry and infirm interaction within the packed nanorods when compared with traditional layered silicates, which gives promise for favorable dispersion in polymer matrix by stirring or ultrasonic vibrations, without one to worry about the intercalation or exfoliation kinetics

H. Yin · H. Chen · D. Chen (✉)
State Key Laboratory for Modification of Chemical Fibers and Polymer Materials, College of Materials Science and Engineering, Donghua University, Shanghai 201620, People's Republic of China
e-mail: cdj@dhu.edu.cn

[10, 11]. What is more, polymer chains may not only interact with the external surface of AT, but also penetrate into its internal channels [12].

Polyacrylonitrile (PAN), an important engineering polymer with widespread commercial applications, has drawn attention in nanocomposite research mainly in two fields: the electrospinning of PAN/silicate nanofiber [13–15] and the in situ polymerization of AN on clay surface and the corresponding morphology control. For example, Fernandez-Saavedra et al. [12] obtained PAN precursor in the nanosized pores of sepiolite and then carbonized into carbon nanofiber. Choi et al. [16] reported synthesis of PAN/Na-MMT nanocomposites via emulsion polymerization, exhibiting the well-exfoliated MMT has great contribution to the storage modulus enhancement of the matrix.

In our recent work, we have reported that the rheological properties of PAN/AT solution and found that small amount of AT nanorods may orient under shear and decrease the viscosity of the solution [17]. Following such a concept, the aim of this study is to investigate the effect of dispersion and motion of AT nanorods on the mechanical properties of PAN/AT nanocomposites. To the best of our knowledge, the corresponding mechanisms have still not yet been comprehensively understood. In this study, both tensile tests and dynamic mechanical analysis (DMA) were performed. The related reinforcement and toughening mechanisms were then proposed based on experimental data and SEM observation of fracture morphology. Also reported is conventional FT-IR results, which objectively show the possible interaction between AT surface and PAN chains. These results and analyses may help explain why the ductility and embrittlement of PAN matrix is dependent on the clay motion and dispersion.

Materials and methods

Materials

Commercial PAN copolymer was purchased from Shanghai Petro-Chemical Company. The copolymer containing ~5 wt% of itaconic acid (IA) was synthesized by a continuous free radical polymerization technique. The weight-average molecular weight (M_w) of the product is in the range of 70,000–80,000 g mol^{-1} and the polydiversity (PDI) of the copolymer is in the range of 3.5–3.8. The pristine AT powder (commercial name "Atta-Gel200") was supplied by Jiangsu Junda Attapulgite Material Co., Ltd. (purity > 90%). A maximum coarseness of AT powder was about 200 mesh. DMSO (analytically pure) was purchased from Shanghai Wulian Chemical Industry Co., Ltd. and deionized water was used in the study.

Preparation of PAN/AT nanocomposites

The crude AT powder was pretreated with hydrogen peroxide solution and stirring with de-ionized water for 12 h. The resulting slurry was then diluted and gravitational sedimentated for 24 h to get rid of impurities. Then the purified AT was treated in 1-mol L^{-1} hydrochloric (HCl) for 5 h to activate hydroxyl groups on AT surface and the suspension was separated through filtration and washed with deionized water until its PH value retained around 7.

Before the nanocomposites preparation, HCl-activated AT powder was dispersed in DMSO using 4-h bath sonication (KUDOS-SK250LH, 59 kHz) at room temperature. Optically homogeneous AT/DMSO dispersion was dropwisely added into PAN/DMSO solutions during stirring through funnel. The nanocomposites were prepared at 60 °C for 8 h and the polymer mass fraction of the solution was controlled at 15 wt%.

The nanocomposite films with 0, 1, 3, 5, and 7 wt% AT, which were named AT0, AT1, AT3, AT5, AT7, were obtained by casting the blend solution on glass substrate and then pressed with another piece of glass to obtain the as-prepared thin film with almost uniform thickness (0.02–0.04 mm). DMSO solvent in the as-prepared film was evaporated in a blast oven at 80 °C for 2 h and then peeling off from the substrate. In order to remove residual DMSO and other unknown impurities on the surface of nanocomposite film, all samples were successively washed by ethanol and then dried in 50 °C vacuum oven for about 30 min.

Characterizations

The tensile tests of the films were performed on universal material tensile machine (WDW, Changchun Greatwall Machine Co., Ltd.). Film samples were diced into strips with 50-mm long and 7-mm width. The tensile speed was 3 mm/min at room temperature with about 65% environmental humidity. At least five samples were tested for each film and the data were averaged. Scanning electron microscopy (HRSEM, Hitachi S-4800) was used to study the morphology of HCl-treated AT. The powder samples were dispersed in isopropanol in an ultrasonic bath for 10 min before HRSEM observations. Fracture surfaces of the neat PAN and nanocomposites films were observed by SEM (JEOL JSM-5600LV) after Pt coating. UV–vis transmittance spectra were obtained using a Perkin-Elmer Lambda 2S UV–vis spectrometer at a wavelength scan rate of 60 nm/min. FT-IR spectra were recorded on a Nicolet 8700 FT-IR spectrometer at a resolution of 4 cm^{-1} by a deuterate triglycine sulfate (DTGS) detector. X-ray diffraction was conducted on a Dmax-2500PC X-ray diffractometer (Rigaku, Japan) with nickel-filtered Cu-K_α

($\lambda = 0.154$ nm) radiation. Each film has been washed and aged at 60 °C oven for 1 h. Dynamic mechanical properties were performed with the film extension mode at frequency of 10 Hz on TA Q800 DMA instruments. The temperature scale of the measurements was set from 30 to 160 °C with a heating rate 2 °C/min.

Results and discussion

Dispersion of AT nanorods in PAN/AT nanocomposites films

Figure 1 is the SEM image of our purified AT. It is clear from this picture that the AT nanorods showed a loose bundle structure after sonication, indicating the exfoliation of AT nanorods is much easier than the previously reported layered clay species. The length of the AT nanorods is not very uniform and varies from 1 μm to several hundred nanometers, while the diameter is about 50 nm.

The state of dispersion of AT in the PAN matrix will be an important factor for the mechanical properties of the nanocomposite. Figure 1b, c, d, and e shows the SEM images of fractured section morphologies of PAN/AT nanocomposites films with 1, 3, 5, and 7 wt% AT, respectively. All samples for the SEM observation were prepared by fracturing in liquid nitrogen. In a wide field of view, it can be found that the AT nanorods are dispersed well but irregularly distributed in the matrix, even in the sample with 7 wt% AT content. Close examination further demonstrates the good wetting ability of AT in the PAN matrix, indicating the surface energies were in favor of AT–PAN contact. Figure 2 shows the UV–vis transmission spectra of pure PAN and the nanocomposites films (wavelength range 250–600 nm). The transmittance of the films monotonically decreases with increasing AT contents, exhibiting the light scattering of the nanofiller in the matrix. More direct evidence comes from the photograph images of the samples (the inset of Fig. 2). One can see that the films gradually changes from colorless to yellow as increasing AT concentration, reflecting the increase of light scattering in the nanocomposites. However, all films still keep the good optical clarity and the words under the film can be clearly discerned, suggesting the well-dispersion uniformity of AT in the matrix [18, 19]. In addition, note that the value of transmittance for all samples is much

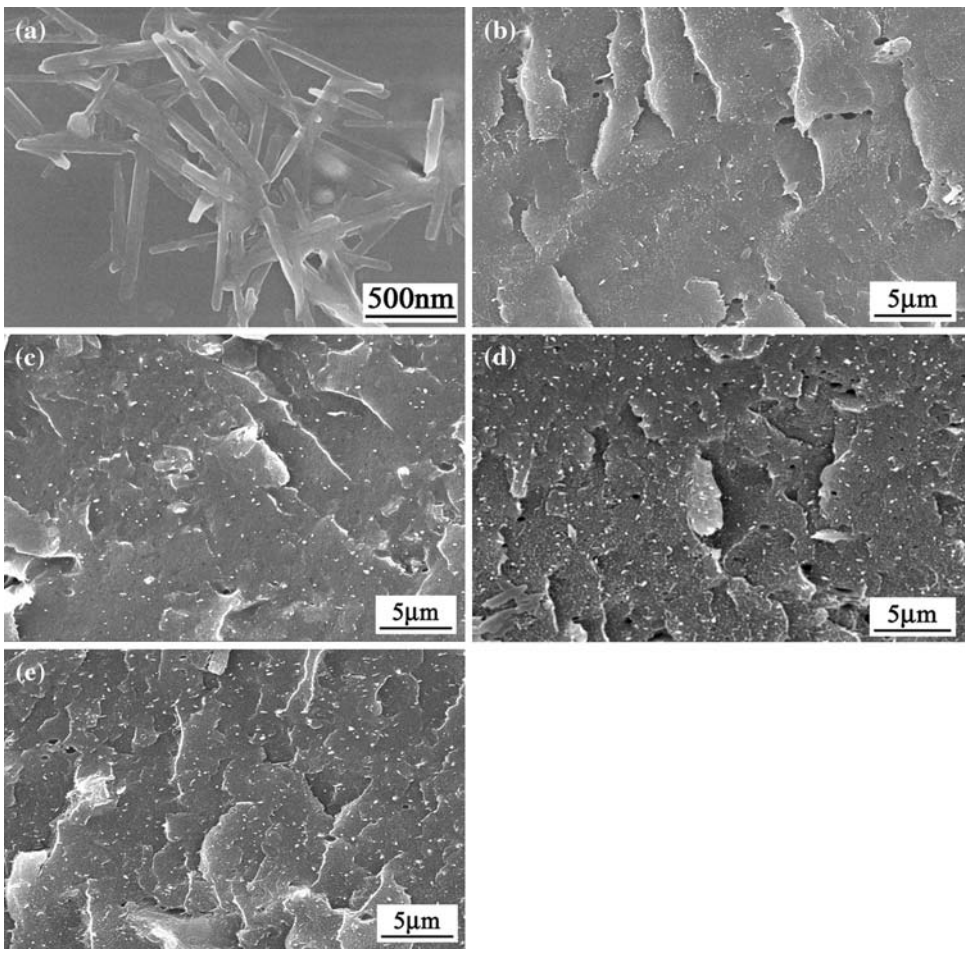

Fig. 1 SEM images of AT and the nanocomposites: **a** HCl-activated AT nanorods (HR-SEM), **b** 1 wt%, **c** 3 wt%, **d** 5 wt%, and **e** 7 wt% AT concentration

higher than that in polymer/layered silicate system [20], further illustrating the light-scattering effect of the rod-like silicates is relatively weak as compared to the layered silicate, probably owing to the geometry differences between two nanofiller species.

Mechanical properties of PAN/AT composite films

Figure 3a demonstrates that the tensile modulus of nanocomposite films monotonically increases as increasing AT content. This result is normal, however, we note that the increase is not linear and the largest modulus appeared when AT content reaches 7 wt%. The effect of AT contents on the tensile strength and the elongation at break are presented in Fig. 3b. The tensile strength and the elongation at break of the neat PAN film in this study were 32 ± 2 MPa and 21 ± 1%, respectively. These two values increase to 49 ± 2 MPa and 26 ± 3% after incorporating 1-wt% AT nanoparticles, corresponding to the improvement of 53 and 24%, respectively. The strain energy at failure (area under the true stress–strain curves) also shows the similar trend, i.e., about 50% increase by addition of 1 wt% of AT nanoparticles (Fig. 3c). Nevertheless, with further increase of AT, the value of tensile strength gradually reduced but still better than that of the pure PAN sample. In addition, further raise of AT content also results in concurrent decrease in both elongation and strain energy at failure, suggesting increasing brittleness of the high-clay-containing samples.

Combining with the previous literatures, we note that the optimal clay content reported here are somehow inconsistent with other polymer/AT systems, such as 4 wt% [10] in PA/AT and 7 wt% in PI/AT nanocomposites [21]. According to the well-known concept that the transfer of the exceptional mechanical properties from nanoscale to macroscale is a crucial point in reinforcement for nanocomposites system and such transfer is generally based on the interfacial bonding between two phases [18], we assume this kind of differences may be caused by different kind of polymer–clay interactions. Therefore, it is

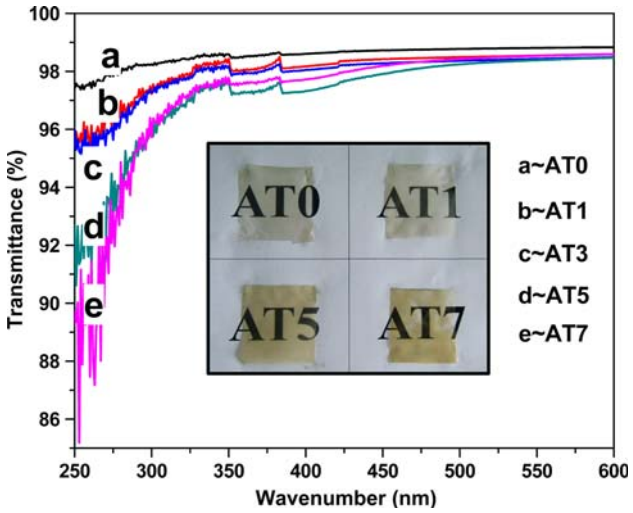

Fig. 2 UV–vis spectra of PAN samples with different AT contents; three scans for each samples were conducted at three different randomly chosen places

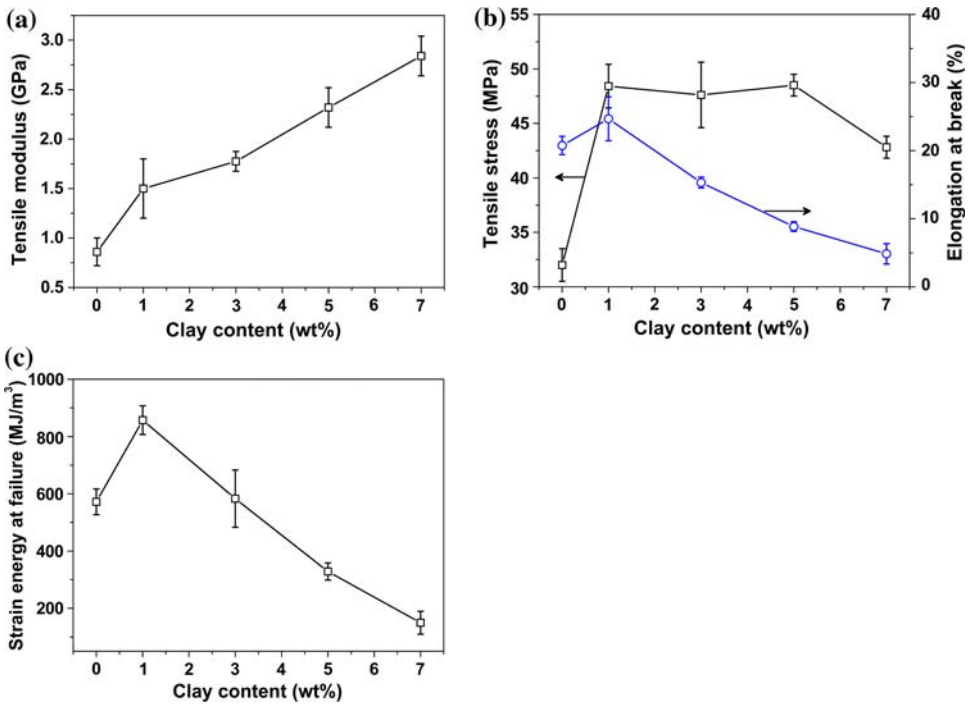

Fig. 3 **a** Tensile modulus, **b** tensile strength and elongation at break of the nanocomposite films, **c** strain energy at failure for PAN and PAN/AT nanocomposites as a function of weight fraction of AT nanoparticles. The average values of several experiments are given and error bars are also marked

necessary to identify the interfacial interaction between AT and PAN matrix and the results will be discussed below.

Interaction between AT surface and the copolymer chains

FT-IR spectroscopy is one of the most powerful tools for characterizing the interactions in polymer/clay nanocomposites. Figure 4 shows the FT-IR spectra of PAN copolymer and the nanocomposites. The peak at 2243 cm^{-1} is a typical –CN vibration [22] and the peak at 1715 cm^{-1} is attributed to the carboxyl groups (C=O) stretching, which confirms the IA in the copolymer [23–25]. With FT-IR spectroscopy, the band (1715 cm^{-1}) is observed to shift to low wavenumber region, as shown in Fig. 4. We believe the shifts are due to H-bonding between –OH of AT and carbonyl of PAN copolymer [26, 27]. This result is also consistent with the conclusion in our previous work [28]. In order to further elucidate this H-bond behavior between AT and PAN molecules, a 'reversed' mixture of AT and PAN with a much higher content of AT than actually used was also prepared by solution blending in DMSO and then dried and grinded into powder (weight ratio of AT/PAN ~ 100/1). In Fig. 5, the bands at 2243 (–CN) and 2923 ($–CH_2$) cm^{-1} suggest that PAN exists in the mixture [25]. The peak at 1651 cm^{-1}, which is associated with the hydroxyl stretching vibrations of zeolitic water [29] in AT, shifts toward lower wavenumber (1628 cm^{-1}), further confirming that the H-bond were formed between proton and oxygen atom of carbonyl in the matrix.

However, it is interesting to find that neither the peak position nor the peak widths show any notable difference for –CN stretching vibration. Compared with the obvious H-bonding behavior illustrated above, we postulate that the interaction between –OH and –CN is not obvious as regards to the strong –CN stretching and dipole–dipole interactions [30].

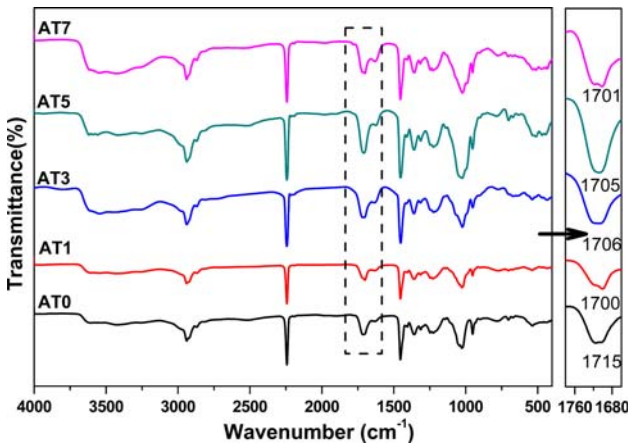

Fig. 4 The FT-IR spectra of neat PAN copolymer and PAN/AT nanocomposites recorded at room temperature

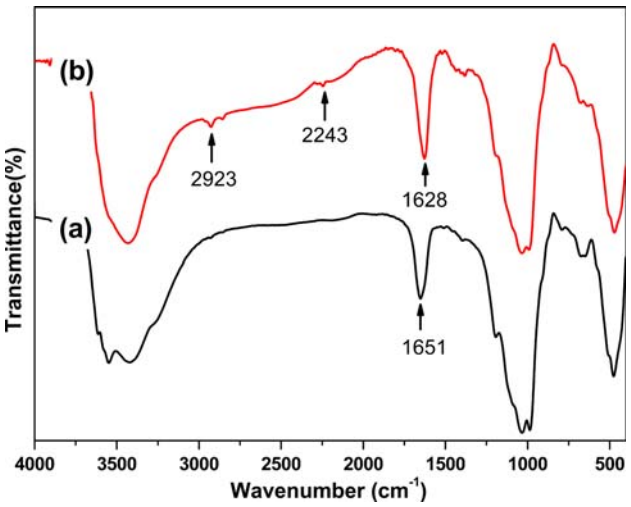

Fig. 5 The FT-IR spectra of (*a*) purified AT and (*b*) AT powder pretreated with diluted PAN solution (weight ratio of AT/PAN ~ 100/1)

Fracture morphology analysis and possible reinforcement/toughening mechanisms

The contribution of the AT nanorods to crack propagation is demonstrated in SEM fractographs of the nanocomposites. In Fig. 6a, one can see a relatively smooth and the typical ductile structure of the neat PAN sample, indicating the cohesive failure happened just prior to final rupture. For the small AT content sample (AT1), the fracture morphology is similar but the surface of specimen becomes a little bit rougher (Fig. 6b). Interestingly, when compared with the morphology of AT stubs in the films that prepared in liquid nitrogen, one may note there are some 'standing' nanorods on the surface (marked by red arrows) and its length and diameters are consistent with size of AT crystal bundles. Therefore, on the basis of tensile results and the morphological observation, we speculate that the cooperative motion of the nanorods and the corresponding crack-pinning effect during stretching are mainly responsible for the improvement of mechanical properties of AT1 sample, especially for the toughness enhancement. The sliding and orientation of small amount of AT nanorods (1 wt% AT in this case) under stretching may result in homogeneous stress transfer and additional path for energy dissipation, hence, increase the value of elongation and the strain energy at failure. However, one point should be mentioned that despite the orientation and mobility of the AT nanorods may play an important role in toughness improvement in this case, the amplitude is much smaller than that reported by Shah et al. [31]. This is probably owing to glassy state of the matrix during mechanical testing. In

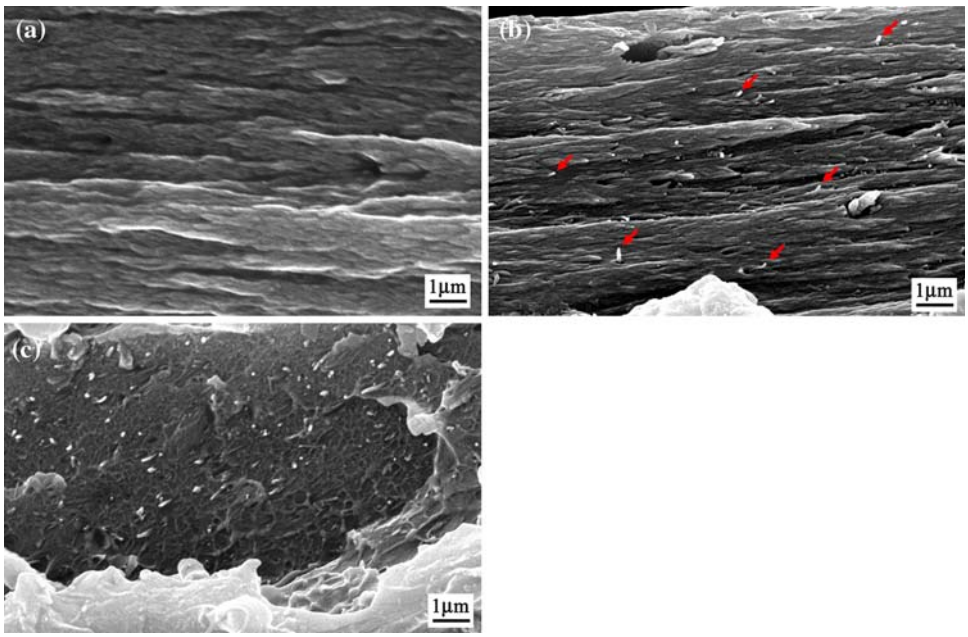

Fig. 6 SEM micrographs of the tensile fracture surface of neat PAN and the nanocomposites: **a** the neat PAN, **b** 1 wt%, **c** 7 wt% AT content

addition, although the H-bond has been verified in our work, we still believe that the interaction is relative weak because of hydrophilic surface of AT nanorods and this also could be one reason for the small amplitude for toughness enhancement.

Besides the mechanism introduced above, another plausible reason for toughness enhancement of AT1 sample is related to the changing of PAN chains conformation. It has been understood that PAN chains seem to take predominantly planar zig-zag and helical conformations in quiescent condition [32] and in PAN/carbon nanotube system, Chae et al. [33] used WXRD to prove that addition of CNT (also the 1-D nanoparticle) in the PAN gel fiber will increase the planar zig-zag sequences of the PAN chains after drawing, probably implying that the motion and orientation of fibrous nanoparticles may accelerate the conformation shifting of PAN chains from helical to planar zig-zag sequences during stretching and consequently contribute to the mechanical properties enhancement. However, this need to be further verified for our system because there is actually no direct evidence for such concept so far.

With further addition of AT nanorods, the morphology of the fracture surface has significantly changed. The ligaments of the matrix could no longer be observed when clay content is 7 wt%. It is also interesting to see that relatively few oriented nanorods (white dot) on the cross-section (Fig. 6c), as compared to the total amount of the clay concentration (7 wt%) in the matrix. The close-up view further demonstrates the 'root-like' network structure of AT nanorods on PAN fracture surface. It is noted that in Fig. 5b the decreasing amplitude of the tensile strength is not as significant as that of the elongation at fracture. Therefore, it can be concluded that this kind of network structure may have more negative effects on the toughness of the matrix than the tensile strength and this result has also illuminated the close relationship between the motion of AT nanorods and the toughness of the matrix.

Furthermore, this kind of network also affects the crystallinity, an important factor for mechanical properties of the matrix [34]. The crystallization degree of PAN/AT nanocomposites has been investigated by XRD and the results are shown in Fig. 7. It can be observed that the location of the characteristic peak position of AT

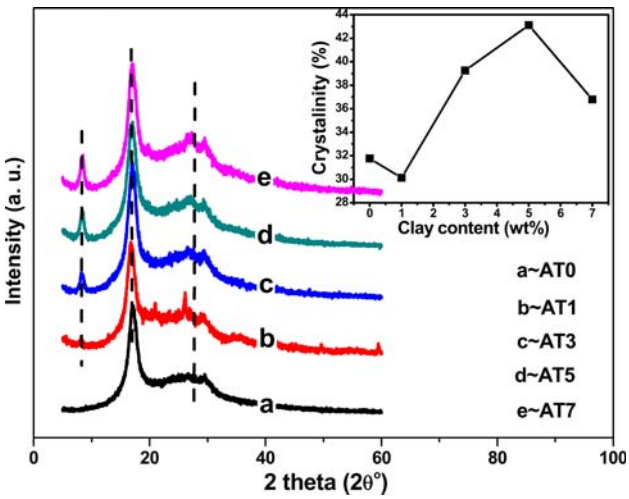

Fig. 7 XRD patterns of neat copolymer and the nanocomposites with different clay concentrations, the *inset* gives the results of crystallinity (%) versus AT content

(110, $2\theta \sim 8°$) in the PAN/AT samples remains unchanged. This is different from layered clay such as montmorillonite, whose diffraction peak shift significantly toward higher/lower theta value when clay aggregated/exfoliated and this difference can be attributed to the different crystal geometry structure. In the spectrum, typical diffraction peak of PAN located at about $2\theta \sim 17°$, which is indexed to (200) crystal plane [35]. The mild peaks $\sim 30°$ correspond to the distortion and irregularity of the crystal structure. The inset of Fig. 7 shows the relationship between clay content and the crystallinity of the nanocomposites. In low AT content sample (AT1–AT5), one may note that the crystallinity generally increases as increasing AT content, indicating the nucleating effect of AT nanorods play the major role in crystallization and this trend is also accordance with the tensile results. However, in the high clay content sample (AT7), the crystallinity shows the downward trend but still better than the neat PAN sample. This decrease may also result from the confinement effect of AT network showed above, which will prevent the motion of polymers chains from fully incorporating into growing crystalline lamella.

It is noteworthy, that although there is no obvious large AT aggregation could be found from SEM photos, we believe the locally dispersed aggregation may still exist in the high AT content matrix, which may lead to microscopic phase segregation [36] and then form weak points during stretching. Therefore, it is safe for us to assume that the main factor for decreasing the tensile strength and ductility in high AT content sample is the clay–clay network structure and clay aggregation induced stress concentration points in the matrix.

DMA of the composites

The DMA is considered to be an efficient method to characterize the network structure in the nanocomposites, especially its damping spectra [37]. The storage moduli (E') versus temperature are shown in Fig. 8a. It can be seen that E' for all nanocomposite samples follow a clear trend, i.e., E' increased with AT content. It is understood that during the glass transition, the long-range polymer chains gain mobility and thus dissipate a great amount of energy through viscous movement and this can be characterized by loss factor (tan δ) (see in Fig. 8b). The temperature of tan δ peak is regarded as the value of T_g (listed in Table 1). When AT content is lower than 3 wt%, it does not change significantly. However, for high AT concentration samples (AT5 and AT7), the peak position moderately shifts toward high temperature and the peak height is depressed. Previous studies on polymer/layered silicates have suggested that the relative heights in T_g dispersions were inversely proportional to the confined polymer segments in the interface layer and the peak height can be used to estimate the amount of constrained chains [38, 39]. In order to quantitatively determine the volume fraction of these regions in PAN/AT nanocomposites, we use the following equations [40–42]:

$$W = \frac{\pi \tan \delta}{\pi \tan \delta + 1} \tag{1}$$

where W is the energy loss fraction in the nanocomposite and the W at tan δ peak is expressed by the dynamic viscoelastic data in the form:

$$W = \frac{(1 - C)W_0}{1 - C_0} \tag{2}$$

where C is the volume fraction of the constrained region, $(1 - C)$ is the fraction of the amorphous region, and the subscript 0 denotes the energy fraction loss and volume fraction of the constrained region for pure PAN, respectively. The energy loss fraction at tan δ peak is obtained at the frequency of 10 Hz and the value of C_0 is assumed to be 0 (assuming totally amorphous phase of

Table 1 T_g Values of PAN and its nanocomposites determined by DMA

Samples	AT0	AT1	AT3	AT5	AT7
T_g (°C)	97.4	99.2	104.9	110.7	111.9

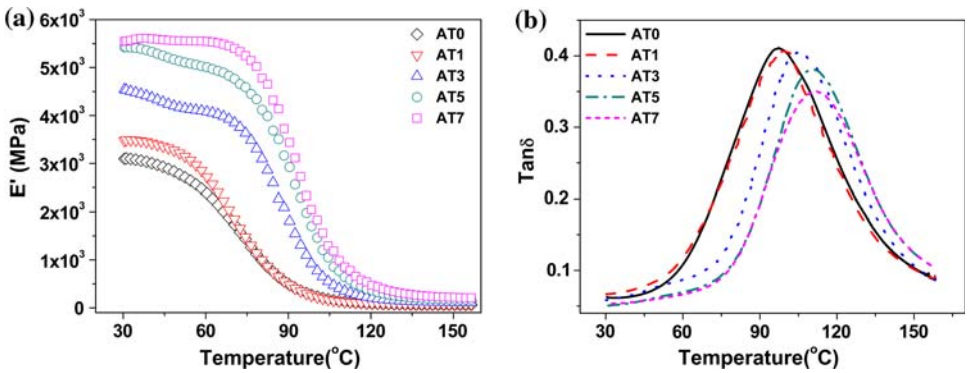

Fig. 8 **a** Storage moduli (E') and **b** loss factor (tan δ) for neat PAN and the nanocomposites

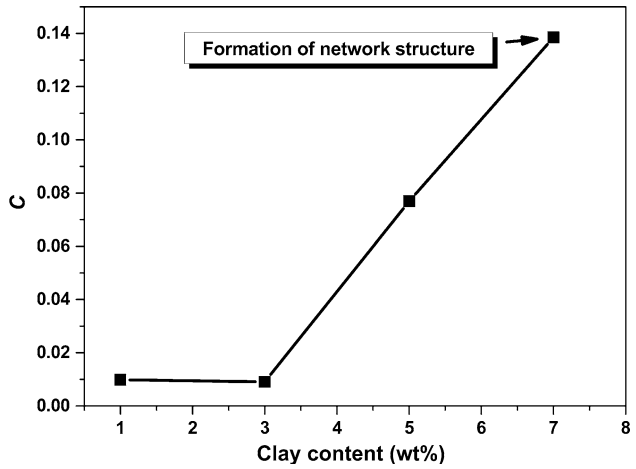

Fig. 9 *C* versus AT content for PAN/AT nanocomposites

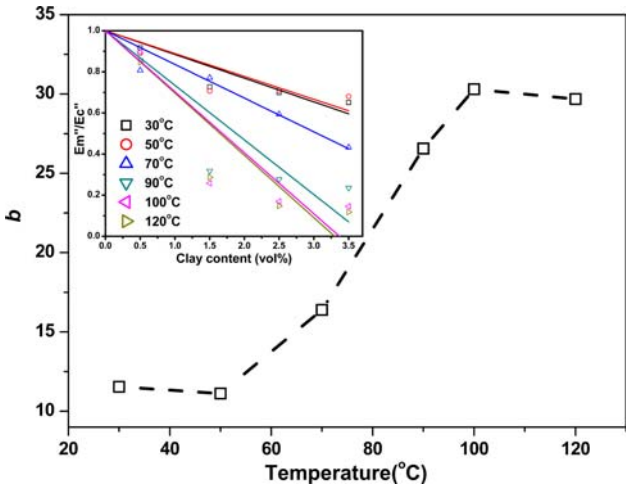

Fig. 10 Effect of temperature on interfacial immobility parameter *b* of the nanocomposites, the *inset* gives the linear fit results of E_c''/E_m'' versus ϕ_f

PAN matrix) [43]. The height of the tan δ peak is used to calculate *W* according to Eq. 1. Figure 9 shows the plots of the volume fraction of the constrained region versus AT content for the PAN/AT systems. It can be seen that for AT7 sample, the volume fraction of the constrained region is much higher than others, indicating that there is much stronger confinement of the PAN chains in AT7 sample and also consistent with the analysis in the tensile modulus and the corresponding SEM photos in Fig. 6c. Furthermore, the relationship between C and AT content is not linear and the critical AT content ϕ_c for clay–clay network can be estimated by Padè-type approximant [43]:

$$\frac{1}{\phi_c} = \frac{7.742 + 14.61x + 12.33x^{3/2} + 1.763x^2 + 1.658x^3}{9.875x + x^2}$$

where *x* is aspect ratio. The value of ϕ_c can be calculated in terms of the densities of PAN: 1.01 g cm^{-3} and AT: 2.0 g cm^{-3} [44]. For the AT nanorods in this work the aspect ratio is $\sim$20, as estimated from Fig. 1a, corresponding to the ϕ_c value of 3.8 vol% or 7.4 wt%. This result suggests that the 7-wt% AT content in our study is the initiating stage of the formation of the percolation structure in the matrix.

One point need to note that the model of chain confinement by AT nanorods seems quite different with the intercalation state of layered silicate or a network model reported by Wang et al. [45]. However, it is difficult to compare the hindrance effect of these two types of nanoparticles because of the difference of interfacial interaction mechanism and particles geometry and the comparison is beyond the scope of this article.

Furthermore, the loss modulus data obtained from the tests can provide the surface adhesion information [46, 47]. An interfacial immobility parameter (semi-empirical), *b*, used to characterize the relative value of the effective volume per volume particles, is shown in Eq. 3.

$$E_c''/E_m'' = (1 - b\phi_f)^{-1} \quad (3)$$

where E_c'' and E_m'' represent the loss module of the composites and the pure polymer during the DMA measurement, respectively, and the ϕ_f represents the volume fraction of fillers. In this article, parameter *b* may represent the surface adhesion between the AT nanorods and the matrix. The value of *b* can be obtained by plotting E_c''/E_m'' versus ϕ_f the linear dependence with fixed intercept 1 (see the inset of Fig. 10). It can be seen that parameter *b* shows a monotonically increase with increasing temperature. It is probably due to the elevated wetting ability between the fillers and matrix under high temperature, for the extent of polymer chains motion becomes easier as temperature rising.

Conclusion

In this article, PAN/AT nanocomposites films with different clay contents were prepared. The mechanical properties of the nanocomposites showed that small amount of AT nanorods ($\sim$1 wt%) in the matrix will concurrently improve both the tensile strength and the toughness of the matrix. FT-IR has further proved that H-bonding was the major interaction between AT and PAN copolymer, which played an important role in stress transfer during stretching. On the basis of fracture morphologies analysis and mechanical tests results, the reinforcement/toughening mechanism has been proposed, showing that the sliding and orientation of small amount of AT nanorods (1 wt% AT in this case) may result to homogeneously stress transfer and energy dissipation during tensile, hence,

increase the mechanical properties of the PAN matrix. However, with increasing particle content to the percolation threshold (5–7 wt%), the motion of the nanorods will be confined from each other and form the clay–clay network structure. Therefore, the plastic deformation of the matrix will be reduced as well as introducing some macroscopic and microscopic stress concentration points to the matrix. The similar conclusion was also obtained from XRD analysis. DMA results demonstrated that both the storage modulus and the T_g values increased as the clay content increasing. The trend of the constrained volumes obtained from the peak height of tan δ was also analogous to that of the tensile modulus. The value of interfacial immobility parameter b that obtained from loss modulus indicated that elevating of temperatures will enhance the interfacial compatibility between AT and the matrix.

Acknowledgements This study was supported by Grants from the National Basic Research Program (973 Program) (No. 2006CB606505), the National Natural Foundation of China (No. 50333050), the Shanghai Fundamental Theory Program (No. 07DJ14002) and the Programme of Introducing Talents of Discipline to Universities (No. 111-2-04) and the Fund of Innovation Project on Doctoral Dissertation of Donghua University.

References

1. Ray SS, Okamoto M (2003) Prog Polym Sci 28:1539
2. Letaief S, Detellier C (2009) Langmuir 25:10975
3. Diaconu G, Micusik M, Bonnefond A, Paulis M, Leiza JR (2009) Macromolecules 42:3316
4. Zhang B, Li YF, Pan XB, Jia X, Wang XL (2007) J Phys Chem Solids 68:135
5. Shen L, Lin YJ, Du QG, Zhong W, Yang YL (2005) Polymer 46:5758
6. Peng ZQ, Chen DJ (2006) J Polym Sci B 44:1995
7. Li A, Wang A (2005) Eur Polym J 41:1630
8. Wang CH, Auad ML, Marcovich NE, Nutt S (2008) J Appl Polym Sci 109:2562
9. Galan E (1996) Clay Miner 31:443
10. Pan BL, Yue QF, Ren JF, Wang HG, Jian LQ, Zhang JY, Yang SR (2006) Polym Test 25:384
11. Tian M, Qu CD, Feng YX, Zhang LQ (2003) J Mater Sci 38:4917. doi:10.1023/B:JMSC.0000004414.27574.93
12. Fernandez-Saavedra R, Aranda P, Ruiz-Hitzky E (2004) Adv Funct Mater 14:77
13. Kedem S, Schmidt J, Paz Y, Cohen Y (2005) Langmuir 21:5600
14. Mack JJ, Viculis LM, Ali A, Luoh R, Yang GL, Hahn HT et al (2005) Adv Mater 17:77
15. Ji LW, Saquing C, Khan SA, Zhang XW (2008) Nanotechnology 19:085605
16. Choi YS, Wang KH, Xu MZ, Chung IJ (2002) Chem Mater 14:2936
17. Yin H, Mo D, Chen DJ (2009) J Polym Sci B 47:945
18. Podsiadlo P, Kaushik AK, Arruda EM, Waas AM, Shim BS et al (2007) Science 318:80
19. Koo CM, Ham HT, Choi MH, Kim SO, Chung IJ (2003) Polymer 44:681
20. Yu YH, Lin CY, Yeh JM, Lin WH (2003) Polymer 44:3553
21. An L, Pan YZ, Shen XW, Lu HB, Yang YL (2008) J Mater Chem 18:4928
22. Coleman MM, Sivy GT (1981) Carbon 19:123
23. Kalagasidis Krušić M, Džunuzović E, Trifunović S, Filipović J (2004) Euro Polym J 40:793
24. Yazdani-Pedram M, Vega H, Quijada R (2001) Polymer 42:4751
25. Ouyang Q, Cheng L, Wang HJ, Li KX (2008) Polym Degrad Stabil 93:1415
26. Benson RS, Lee MW, Grummitt DW (1995) Nanostruct Mater 6:83
27. Dai XH, Xu J, Guo XL, Lu YL et al (2004) Macromolecules 37:5615
28. Yin H, Chen HF, Chen DJ (2010) Polym Eng Sci. doi: 10.1002/pen.21550
29. Huang JH, Liu YF, Jin QZ, Wang XG (2007) Spectrosc Spect Anal 27:408
30. Lachat V, Varshney V, Dhinojwala A, Yeganeh MS (2009) Macromolecules 42:7103
31. Shah D, Maiti P, Jiang DD, Batt CA, Giannelis EP (2005) Adv Mater 17:525
32. Liu XD, Ruland W (1993) Macromolecules 26:3030
33. Chae HG, Minus ML, Kumar S (2006) Polymer 47:3494
34. Gopakumar TG, Lee JA, Kontopoulou M, Parent JS (2002) Polymer 43:5483
35. Hou HQ, Ge JJ, Zeng J, Li Q et al (2005) Chem Mater 17:967
36. Mackay ME, Tuteja A, Duxbury PM, Hawker CJ, Van Horn B et al (2006) Science 311:1740
37. Pan YZ, Xu Y, An L, Lu HB, Yang YL, Chen W, Nutt S (2008) Macromolecules 41:9245
38. Burnside SD, Giannelis EP (2000) J Polym Sci B 38:1595
39. Abdalla M, Dean D, Adibempe D, Nyairo E, Robinson P, Thompson G (2007) Polymer 48:5662
40. Kojima Y, Usuki A, Kawasumi M, Okada A, Kurauchi T, Kamigaito O (1993) J Appl Polym Sci 49:1259
41. Kojima Y, Usuki A, Kawasumi M, Okada A, Fukushima Y, Kurauchi T, Kamigaito O (1993) J Mater Res 8:1185
42. Zhang XH, Loo LS (2009) Macromolecules 42:5196
43. Garboczi EJ, Snyder KA, Douglas JF (1995) Phys Rev E 52:819
44. Guo HN, Sreekumara TV, Liu T, Minusa M, Kumar S (2005) Polymer 46:3001
45. Wang K, Liang S, Deng JN, Yang H, Zhang Q et al (2006) Polymer 47:7131
46. Sumit M, Tsukihi H, Miyasaka K, Ishikawa K (1984) J Appl Polym Sci 29:1523
47. Sun SS, Li CZ, Zhang L, Du HL, Burnell-Gray JS (2006) Eur Polym J 42:1643